# Erythrocyte membrane-camouflaged polymeric nanoparticles as a biomimetic delivery platform

Che-Ming J. Hu, Li Zhang, Santosh Aryal, Connie Cheung, Ronnie H. Fang, and Liangfang Zhang[1]

Department of NanoEngineering and Moores Cancer Center, University of California, San Diego, La Jolla, CA 92093

Edited by Omid C. Farokhzad, Brigham and Women's Hospital, Harvard Medical School, Boston, MA, and accepted by the Editorial Board May 24, 2011 (received for review April 26, 2011)

**Efforts to extend nanoparticle residence time in vivo have inspired many strategies in particle surface modifications to bypass macrophage uptake and systemic clearance. Here we report a top-down biomimetic approach in particle functionalization by coating biodegradable polymeric nanoparticles with natural erythrocyte membranes, including both membrane lipids and associated membrane proteins for long-circulating cargo delivery. The structure, size and surface zeta potential, and protein contents of the erythrocyte membrane-coated nanoparticles were verified using transmission electron microscopy, dynamic light scattering, and gel electrophoresis, respectively. Mice injections with fluorophore-loaded nanoparticles revealed superior circulation half-life by the erythrocyte-mimicking nanoparticles as compared to control particles coated with the state-of-the-art synthetic stealth materials. Biodistribution study revealed significant particle retention in the blood 72 h following the particle injection. The translocation of natural cellular membranes, their associated proteins, and the corresponding functionalities to the surface of synthetic particles represents a unique approach in nanoparticle functionalization.**

biomimetic nanoparticle | drug delivery | long circulation | red blood cell membrane

Long-circulating polymeric nanoparticles have significant clinical impact as they promise sustained systemic delivery and better targeting through both passive and active mechanisms (1–3). Different approaches including modifications on particle size, surface, shape, and flexibility have been explored to extend particle residence time in vivo (4–6). The current gold standard for nanoparticle stealth coating is PEG. The adoption of PEG as a stealth moiety on nanoparticle surface has led to great success with several clinical products (2, 3), but recent observation of anti-PEG immunological response has triggered the interest of further investigation on its biological relevance (7). Synthetic zwitterionic materials such as poly(carboxybetaine) and poly(sulfobetaine) have been proposed as alternatives to PEG because of their strong hydration that is highly resistant to nonspecific protein adsorption (8, 9). In addition, recent advances in molecular and cellular biology have inspired scientists and nanotechnologists to model nanocarriers after RBCs, which are nature's long-circulating delivery vehicles. Properties of RBCs such as their structure and surface proteins have been taken as design cues to devise the next-generation delivery platforms (10–12).

Although significant efforts have been devoted to bridging the gap between synthetic nanomaterials and biological entities, an RBC-mimicking delivery vehicle has remained elusive to biomedical researchers. One major challenge lies in the difficulty in functionalizing nanoparticles with the complex surface chemistry of a biological cell. Despite the recent great progress in reducing macrophage engulfment of polystyrene beads following their conjugation with an immunosuppressive RBC-membrane protein, CD47 (11), current chemistry-based bioconjugation techniques often lead to protein denaturation. In addition, these bottom-up approaches are largely inadequate in duplicating a complex protein makeup on a nanoscale substrate. Inspired by the concept of bridging synthetic and natural materials and by the need to reinvent nanoparticle functionalization, we herein develop an RBC-membrane-camouflaged polymeric nanoparticle platform through a top-down method. By extruding poly(lactic-co-glycolic acid) (PLGA) particles with preformed RBC-membrane-derived vesicles, we coat the sub-100-nm polymeric particles with the bilayered RBC membranes including both lipids and the corresponding surface proteins. This approach aims to camouflage the nanoparticle surface with the erythrocyte exterior for long circulation while retaining the applicability of the polymeric core. We report the physical characterizations, physicochemical properties, protein contents, pharmacokinetics, and biodistribution of this biomimetic nanoparticle delivery platform.

## Results and Discussion

The preparation process of the RBC-membrane-coated nanoparticles is divided into two parts: membrane vesicle derivation from RBCs and vesicle-particle fusion (Fig. 1). The derivation of RBC-membrane vesicles follows a previously reported method with slight modifications (13). Briefly, RBCs were first purified from the fresh blood of male Imprinting Control Region (ICR) mice (6–8 wk) from Charles River Laboratories by centrifugation and PBS wash. The isolated RBCs then underwent membrane rupture in a hypotonic environment to remove its intracellular contents. Next, the emptied RBCs were washed and extruded through 100-nm porous membranes to create RBC-membrane-derived vesicles. To synthesize the RBC-membrane-camouflaged polymeric nanoparticles, PLGA particles of approximately 70 nm in diameter were first prepared from 0.67 dL/g carboxyl-terminated PLGA polymer using a solvent displacement method (14). The resulting PLGA nanoparticles were subsequently fused with the RBC-membrane-derived vesicles through mechanical extrusion. Based on calculations from PLGA polymer density, nanoparticle size, the erythrocyte lipid contents, and the estimated project area of a lipid molecule, each milligram of PLGA nanoparticles was mixed with vesicles derived from 1 mL of blood for complete particle coating. The mixture was physically extruded through an apparatus with 100-nm pores. The mechanical force facilitated the sub-100-nm PLGA nanoparticles to cross the lipid bilayers, resulting in vesicle-particle fusion. Repeated passing through the extruder overcomes previously reported issues with liposome-particle fusion, such as broad particle size distribution, incomplete particle coating, and inconsistent lipid shells (15). It should also be noted that the bilayer structure of the RBC membranes is retained throughout the entire preparation process to minimize the loss of and damages to the membrane proteins.

Author contributions: C.-M.J.H., Li Zhang, and Liangfang Zhang designed research; C.-M.J.H., Li Zhang, S.A., C.C., and R.F. performed research; C.-M.J.H., Li Zhang, S.A., C.C., R.F., and Liangfang Zhang analyzed data; and C.-M.J.H. and Liangfang Zhang wrote the paper.

The authors declare no conflict of interest.

This article is a PNAS Direct Submission. O.C.F. is a guest editor invited by the Editorial Board.

[1]To whom correspondence should be addressed. E-mail: zhang@ucsd.edu.

This article contains supporting information online at www.pnas.org/lookup/suppl/doi:10.1073/pnas.1106634108/-/DCSupplemental.

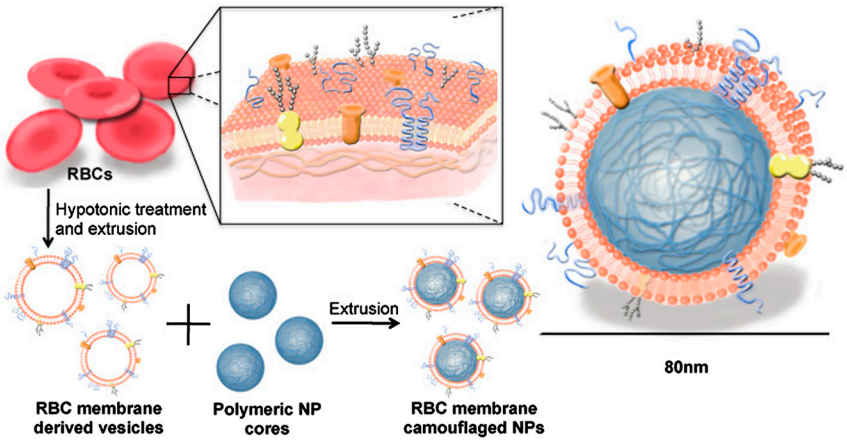


**Fig. 1.** Schematics of the preparation process of the RBC-membrane-coated PLGA nanoparticles (NPs).

To characterize the RBC-membrane-coated PLGA nanoparticles, the particles were first negatively stained with uranyl acetate and then visualized using transmission electron microscopy (TEM) (Fig. 2*A*). The resulting image reveals a core-shell structure as expected in a lipid bilayer-coated polymeric particle. The particle size is approximately 80 nm and matches the hydrodynamic diameter measured by dynamic light scattering (DLS). Closer examination reveals a polymeric core approximately 70 nm in diameter and an outer lipid shell 7–8 nm in thickness. The thickness of the lipid layer is in agreement with the reported membrane width of RBCs (16), suggesting a successful membrane translocation to the polymeric particle surface.

To examine the long-term stability of the resulting RBC-mimicking nanoparticles, they were suspended in 1× PBS at a concentration of 1 mg/mL and then monitored by DLS for the particle size, the polydispersity index (PDI), and the surface zeta potential (Fig. 2*B*). Over a span of two weeks the particle size increased from 85 to 130 nm, the zeta potential decreased from −10.2 to −12.7 mV, and the PDI remained relatively the same at 0.26. The changes in size and zeta potential are likely caused by the fusion of small amount of excess vesicles in the particle solution. To verify the integrity of the core-shell particle structure, hydrophobic 1,1′-dioctadecyl-3,3,3′,3′-tetramethylindodicarbocyanine, 4-chlorobenzenesulfonate salt (DiD) fluorophore (excitation/emission = 644 nm/655 nm) and the lipophilic 1,2-dimyristoyl-sn-glycero-3-phosphoethanolamine-N-(lissamine rhodamine B sulfonyl) (ammonium salt) (DMPE-RhB) fluorophore (excitation/emission = 557 nm/571 nm) were loaded into the polymeric core and the RBC-membrane-derived vesicles, respectively, prior to the vesicle-particle fusion. The resulting dual-fluorophore-labeled nanoparticles were incubated with HeLa cells for 6 h and visualized using fluorescence microscopy. In Fig. 2*C*, DiD (red) and rhodamine-DMPE (green), each of which corresponds to a different particle compartment, overlap in the same locations. This fluorescence colocalization indicates an intact core-shell structure of the nanoparticles after they are internalized by the cells.

Following the structural studies, the particles were examined for their protein contents. The RBC-membrane-coated nanoparticles were dialyzed with 30-nm porous membranes for 24 h to remove unbound proteins and subsequently treated with SDS to solubilize the membrane proteins. Samples of emptied RBCs and RBC-membrane-derived vesicles were prepared in parallel as a comparison. Protein separation by PAGE indicates that the composition of membrane proteins was mostly retained throughout the particle synthesis and can be identified on the RBC-membrane-coated PLGA nanoparticles (Fig. 3*A*). This finding suggests that the translocation of the bilayered cellular membranes also transfers the associated membrane proteins to the nanoparticle surface. Because the solid PLGA core precludes protein entries and unbound proteins are filtered out by dialysis, the detected membrane proteins are most likely anchored in the bilayered lipid membranes that surround the nanoparticles. The resulting protein-containing lipid membrane-coated particles can be likened to a well-studied polymer-supported planar lipid bilayer model, which has been shown to retain the functionalities of membrane-associated proteins (15). Minor alteration in the protein makeup, however, was observed as a band near 51 kDa is noticeably fainter. The faint band likely corresponds to peripheral membrane proteins associated with spectrin cytoskeletal proteins, which are lost during the mechanical extrusion for the vesicle-particle fusion as can be observed by the missing band at approximately 200 kDa.

We then investigated the serum stability and the in vivo circulation half-life of the RBC-membrane-coated nanoparticles. To put the results into perspective, similarly sized bare PLGA nanoparticles (approximately 75 nm) and structurally analogous PEG 2000-functionalized lipid-polymer hybrid nanoparticles (approximately 80 nm) were used as negative and positive controls, respectively. For the serum stability test, a previously cited absorbance method was used to monitor the particle size change in the presence of FBS (17, 18). Because larger particles induce higher light scattering, aggregation of unstable particles can be observed by monitoring the increase in the absorbance value. Each type of nanoparticle was suspended in 100% FBS with a final nanoparticle concentration of 1 mg/mL. All samples were incubated at 37 °C and shaken gently prior to each absorbance measurement. The absorbance values measured at 560 nm suggest that the RBC-membrane-coated nanoparticles have equivalent serum stability as the PEG-functionalized lipid-polymer hybrid nanoparticles as neither sample showed any observable change in absorbance within 4 h (Fig. 3*B*). In contrast, the bare PLGA nanoparticles showed little stability as they immediately aggregated upon mixture with the serum solution.

To study the systemic circulation time of each type of nanoparticle, we loaded the hydrophobic DiD fluorescent dye to all three types of nanoparticles. The dye shows minimal release (<20% in 72 h) and has been widely cited as a marker for the circulation studies of nanoparticles (19, 20). For each particle type, 150 μL of 3 mg/mL DiD-loaded nanoparticles were injected into a group of six mice through tail-vein injection. To avoid the immune responses associated with different blood types, the mice subject to the circulation studies are of the same strain from which the RBCs are collected to prepare the nanoparticles. At various time points following the injection, 20 μL of blood were collected from the eye socket of the mice for fluorescence measurements. Fig. 3*C* shows that the RBC-membrane-coated nanoparticles had super-

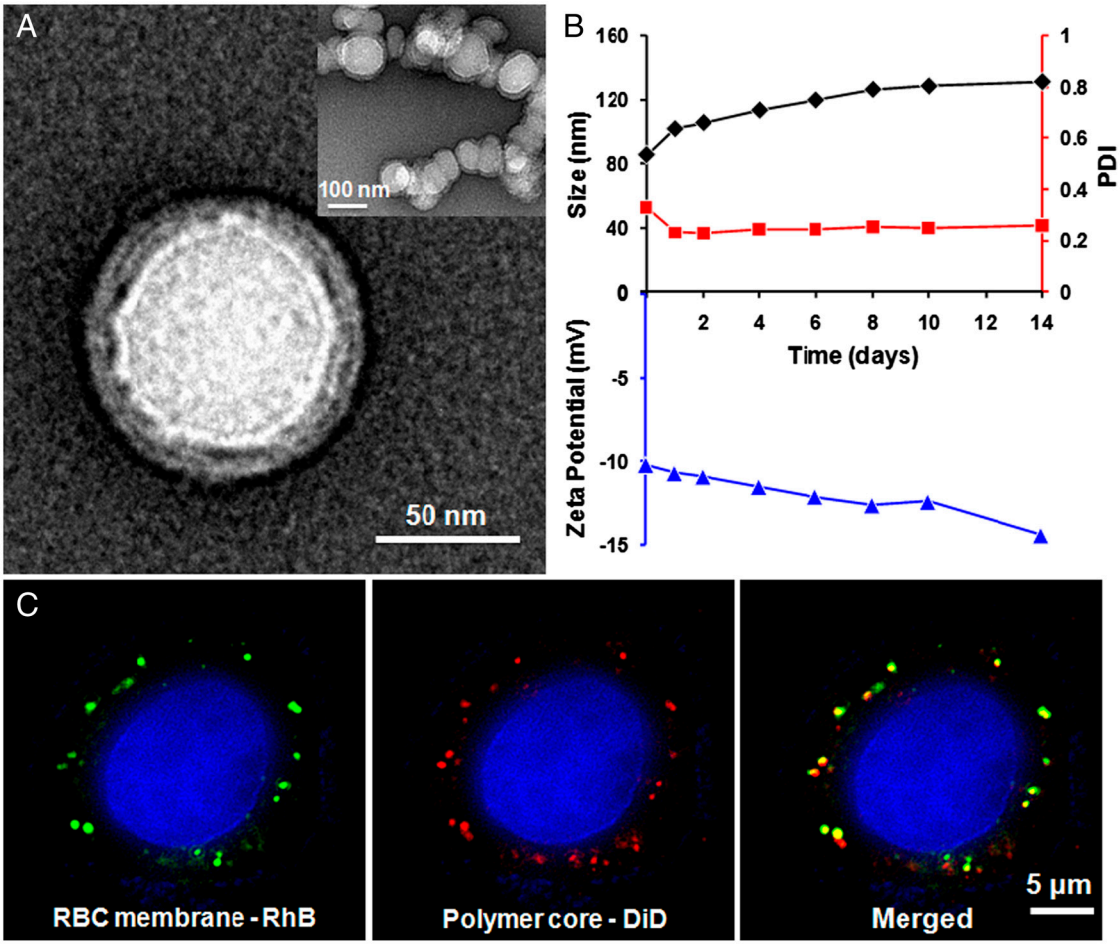


**Fig. 2.** Structural characterization of the RBC-membrane-coated PLGA nanoparticles. (*A*) The nanoparticles were negatively stained with uranyl acetate and subsequently visualized with TEM. (*B*) DLS measurements of the size, PDI, and surface zeta potential of the nanoparticles over 14 d. (*C*) Scanning fluorescence microscopy images demonstrated the colocalization of the RBC membranes (visualized with green rhodamine-DMPE dyes) and polymeric cores (visualized with red DiD dyes) after being internalized by HeLa cells. The RBC-membrane-coated nanoparticles were incubated with HeLa cells for 6 h. The excess nanoparticles were washed out, and the cells were subsequently fixed for imaging.

ior blood retention to the PEG-functionalized nanoparticles. At 24- and 48-h marks, the RBC-membrane-coated nanoparticles exhibited 29% and 16% overall retention, respectively, as compared to the 11% and 2% exhibited by the PEG-coated nanoparticles. The bare PLGA nanoparticles, on the other hand, showed negligible signal in the first blood withdrawal at the 2-min mark, which was expected based on their rapid aggregations in serum. The semilog plot in Fig. 3*C*, *Inset*, better illustrates the difference in the pharmacokinetic profiles as circulation half-life can be derived from the slope of the semilog signals. Based on a two-compartment model that has been applied in previous studies to fit the circulation results of nanoparticles (21, 22), the elimination half-life was calculated as 39.6 h for the RBC-membrane-coated nanoparticles and 15.8 h for the PEG-coated nanoparticles. Alternatively, the circulation data in Fig. 3*C* can be interpreted through a one-way nonlinear clearance model, where the causes of nanoparticle clearance (i.e., availability of clearing sites and opsonin proteins) are continuously depleted to give rise to a slowing particle uptake. Simberg et al. have reported that by injecting "decoy" particles prior to the injection of primary particles, the circulation half-life of the primary particles can be prolonged by nearly 5-fold (23). It is reasonable to expect that the saturation of the reticuloendothelial system (RES) can retard additional particle uptake and account for a nonlinear particle elimination rate. Based on this nonlinear elimination model, the first apparent half-life (i.e., 50% of the particles are cleared) is 9.6 h for the RBC-membrane-coated nanoparticles and 6.5 h for the PEG-coated nanoparticles. Regardless of the pharmacokinetic models, the RBC-membrane-coated nanoparticles have longer elimination half-life, which suggests that the RBC-membrane coating is superior in retarding in vivo clearance compared to the conventional PEG stealth coating. This finding further confirms that the nanoparticles were modified with the functional components on the RBC membranes, which contain immunosuppressive proteins that inhibit macrophage uptake (24). Because these membrane proteins are from the natural RBCs collected from the host blood, they are expected to stimulate negligible immune response after they are translocated to the surface of polymeric nanoparticles. With the TEM visualization, the SDS-PAGE results, and the circulation half-life study, we demonstrate the transfer of cell membranes and the corresponding functional surface proteins for nanoparticle functionalization using the reported technique.

Finally we investigated the in vivo tissue distribution of the RBC-membrane-coated nanoparticles to further evaluate their potential as a delivery vehicle. For the biodistribution study, 18 mice received an injection of 150 μL of 3 mg/mL DiD-loaded nanoparticles through the tail vein. At each of the 24-, 48-, and 72-h time points following the particle injection, six mice were euthanized and their livers, kidneys, spleens, brains, lungs, hearts, and blood were collected. For fluorescence quantification, the organs collected at different time points were washed, weighed, homogenized in 1 mL PBS, and then measured by a fluorospectrometer. Fig. 4*A* shows the nanoparticle content per gram of tissue. The two primary organs of the RES, liver and spleen,

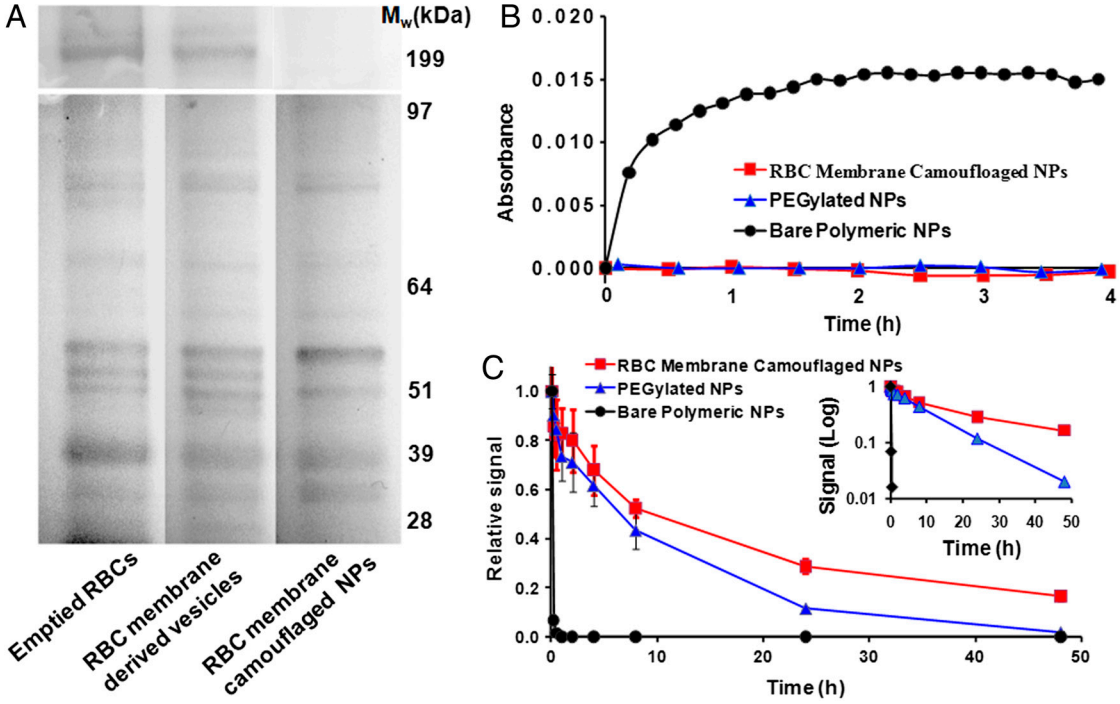


**Fig. 3.** Membrane protein retention, particle stability in serum, and the in vivo circulation time of the RBC-membrane-coated NPs. (*A*) Proteins in emptied RBCs, RBC-membrane-derived vesicles, and purified RBC-membrane-coated PLGA nanoparticles were solubilized and resolved on a polyacrylamide gel. (*B*) RBC-membrane-coated PLGA nanoparticles, PEG-coated lipid-PLGA hybrid nanoparticles, and bare PLGA nanoparticles were incubated in 100% fetal bovine serum and monitored for absorbance at 560 nm for 4 h. (*C*) DiD-loaded nanoparticles were injected intravenously through the tail vein of mice. At various time points blood was withdrawn intraorbitally and measured for fluorescence at 670 nm to evaluate the systemic circulation lifetime of the nanoparticles ($n = 6$ per group).

contained the highest amount of nanoparticles. However, significant fluorescence level was also observed in the blood at the three time points. To better understand the overall particle distribution, the fluorescence signals were multiplied by the measured weight of the corresponding organs, with the weight of the blood being estimated as 6% of the total body weight. Fig. 4*B* shows the relative signal in each organ normalized to the total fluorescence. After accounting for the tissue mass, it can be observed that the nanoparticles are distributed mainly in the blood and the liver. The fluorescence signals from the blood correlate well with the data from the circulation half-life study, with 21%, 15%, and 11% of nanoparticle retention at 24-, 48-, and 72-h marks, respectively. Also, as the blood fluorescence decreased, a corresponding increase in signal was observed in the liver, which indicates that the source of the fluorescence in the blood was eventually taken up by the RES. This result validates that the observed blood fluorescence came from the long-circulating nanoparticles rather than leakage of the dye, which would be secreted by the kidneys and result in a reduction in the signal intensity from the liver. It is worth noting that the RBC-membrane-coated polymeric nanoparticles have a significantly longer circulation time compared to previously reported RBC-derived liposomes, which are cleared from the blood circulation in less than 30 min (13). This prolonged circulation time by the RBC-membrane-coated nanoparticles can be attributed to the higher structural rigidity, better particle stability, and the more reliable cargo/dye encapsulation. As compared to other published data on nanoparticle circulations in mice models (14, 25, 26), most of which show negligible blood retention after 24 h, the RBC-membrane-coated nanoparticles exhibit superior in vivo residence time and hold tremendous potentials for biomedical applications as a robust delivery platform.

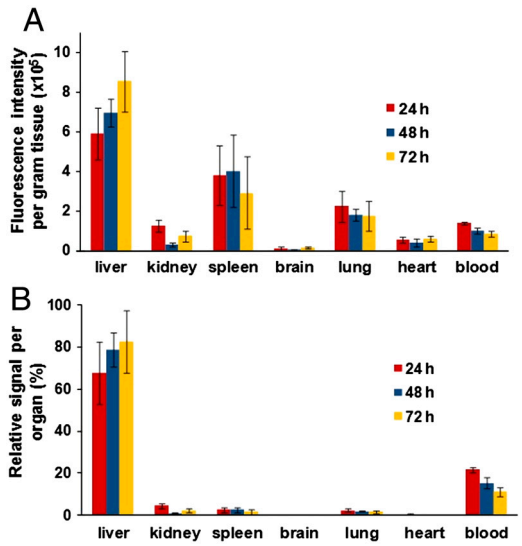


**Fig. 4.** Biodistribution of the RBC-membrane-coated polymeric nanoparticles. Fluorescently labeled nanoparticles were injected intravenously into the mice. At each time point (24, 48, and 72 h respectively), the organs from a randomly grouped subset of mice were collected, homogenized, and quantified for fluorescence. (*A*) Fluorescence intensity per gram of tissue ($n = 6$ per group). (*B*) Relative signal per organ.

The erythrocyte membrane-coated nanoparticles reported herein are structurally analogous to the commonly cited lipid-polymer hybrid nanoparticles, which are quickly emerging as a promising multifunctional drug delivery platform that contains the desirable characteristics of both liposomes and polymeric nanoparticles (27, 28). Lipid-polymer hybrid nanoparticles have shown a more sustained drug release profile compared to polymeric nanoparticles with similar size owing to the diffusional barrier provided by the lipid monolayer coating. The drug release kinetics from the RBC-membrane-coated nanoparticles is ex-

pected to be even more gradual because the RBC membrane provides a more dense and bilayered lipid barrier against drug diffusion. The membrane coating approach in this study can also be extended to other nanostructures as the versatility of lipid coating has made its way to silica nanoparticles and quantum dots (29–31). Further particle functionalization can be achieved by inserting modified lipids, lipid derivatives, or transmembrane proteins to the lipid membranes prior to the preparation of the RBC-membrane-coated nanostructures.

Regarding the translation of these RBC-membrane-coated nanoparticles as a clinical drug delivery vehicle, many challenges and opportunities lie ahead. Unlike in animal studies, human erythrocytes contain numerous surface antigens that can be classified to many different blood groups. To optimize the particles for long-circulating drug delivery, the particles need to be cross-matched to patients' blood as in the case of blood transfusion. For more versatile applications to broad populations of patients, the particles can be selectively depleted of those immunogenic proteins during the synthesis steps. Alternatively, this biomimetic delivery platform could be an elegant method for personalized medicine whereby the drug delivery nanocarrier is tailored to individual patients with little risk of immunogenicity by using their own RBC membranes as the particle coatings.

## Conclusions

In conclusion, we demonstrate the synthesis of an erythrocyte membrane-camouflaged polymeric nanoparticle for long-circulating cargo delivery. The adopted technique aims to fabricate cell-mimicking nanoparticles through a top-down approach that bypasses the labor-intensive processes of protein identifications, purifications, and conjugations. The proposed method also provides a bilayered medium for transmembrane protein anchorage and avoids chemical modifications that could compromise the integrity and functionalities of target proteins. We demonstrate that the lipid layer can be derived directly from live cells. The translocation of natural cellular membranes and their associated functionalities to the particle surface represents a unique and robust top-down approach in nanoparticle functionalization.

## Materials and Methods

**RBC Ghost Derivation.** RBC ghosts devoid of cytoplasmic contents were prepared following previously published protocols with modifications (32). Whole blood was first withdrawn from male ICR mice (6–8 w) obtained from Charles River Laboratories through cardiac puncture using a syringe containing a drop of heparin solution (Cole-Parmer). The whole blood was then centrifuged at 800 × *g* for 5 min at 4 °C, following which the serum and the buffy coat were carefully removed. The resulting packed RBCs were washed in ice cold 1× PBS prior to hypotonic medium treatment for hemolysis. The washed RBCs were suspended in 0.25× PBS in an ice bath for 20 min and were centrifuged at 800 × *g* for 5 min. The hemoglobin was removed, whereas the pink pellet was collected. The resulting RBC ghosts were verified using phase contrast microscopy, which revealed an intact cellular structure with an altered cellular content (Fig. S1).

**Preparation of RBC-Membrane-Derived Vesicles.** The collected RBC ghosts were sonicated in a capped glass vial for 5 min using a FS30D bath sonicator (Fisher Scientific) at a frequency of 42 kHz and power of 100 W. The resulting vesicles were subsequently extruded serially through 400-nm and then 100-nm polycarbonate porous membranes using an Avanti mini extruder (Avanti Polar Lipids). To visualize the liposomal compartment in the RBC-membrane-derived vesicles, 1 mL of whole blood was mixed with 20 μg of DMPE-RhB (Avanti Polar Lipids) during the vesicle preparation process. The size of the RBC-membrane-derived vesicles was measured by DLS after each preparation step (Fig. S2).

**Preparation of PLGA Nanoparticles.** The PLGA polymeric cores were prepared using 0.67 dL/g carboxy-terminated 50:50 poly($_{DL}$-lactide-co-glycolide) (LACTEL Absorbable Polymers) in a solvent displacement process. The PLGA polymer was first dissolved in acetone at a 1 mg/mL concentration. To make 1 mg of PLGA nanoparticles, 1 mL of the solution was added dropwise to 3 mL of water. The mixture was then stirred in open air for 2 h. The resulting nanoparticle solution was filtered with 10 K molecular weight cutoff (MWCO) Amicon Ultra-4 Centrifugal Filters (Millipore) and resuspended in 1 mL PBS (1×, pH = 7.4). For fluorescence microscopy imaging and in vivo particle tracking purposes, 2 μg of 1,1′-dioctadecyl-3,3,3′,3′-tetramethylindodicarbocyanine, 4-chlorobenzenesulfonate salt (DiD) dye (Invitrogen) were added to the PLGA acetone solution prior to PLGA nanoparticle synthesis. The release of DiD dye from PLGA nanoparticles was examined using a dialysis method in which 100 μL of the prepared nanoparticle solutions were loaded into a Slide-A-Lyzer MINI dialysis microtube with a MWCO of 3.5 kDa (Pierce). The nanoparticles were dialyzed in PBS buffer at 37 °C. The PBS solution was changed every 12 h during the dialysis process. At each predetermined time point, nanoparticle solutions from three minidialysis units were collected separately for dye quantification using an Infinite M200 multiplate reader (TeCan) (Fig. S3). As a control particle, the PEG-coated lipid-PLGA hybrid nanoparticles were prepared through a nanoprecipitation method exactly following a previously published protocol (33).

**Fusion of RBC-Membrane-Derived Vesicles with PLGA Nanoparticles.** To fuse the RBC-membrane-derived vesicles with the PLGA nanoparticles, 1 mg of PLGA nanoparticles was mixed with RBC-membrane-derived vesicles prepared from 1 mL of whole blood and then extruded 7 times through a 100-nm polycarbonate porous membrane using an Avanti mini extruder. The mixture ratio was estimated based on the membrane volume of RBCs and the total membrane volume required to fully coat 1 mg of PLGA nanoparticles. Parameters used for the estimation include mean surface area of mouse RBCs (75 $\mu m^2$) (34), membrane thickness of RBC (7 nm), density of 50:50 PLGA nanoparticles (1.34 $g/cm^3$) (35), red blood cell concentration in mouse blood (7 billion per mL) (36), and the mean particle size as measured by DLS before and after the RBC-membrane coating (Fig. S4). An excess of blood was used to compensate for the membrane loss during RBC ghost derivation and extrusion. The resulting RBC-membrane-coated PLGA nanoparticles were dialyzed against 30-nm porous membranes (Avanti Polar Lipids) for 24 h and concentrated through nitrogen purging. The particle size and polydispersity remained identical following dialysis and concentration.

**Characterization of RBC-Membrane-Coated PLGA Nanoparticles.** Nanoparticle size (diameter, nm), polydispersity, and surface charge (zeta potential, mV) were measured by DLS using Nano-ZS, model ZEN3600. Nanoparticles (approximately 500 μg) were suspended in 1× PBS (approximately 1 mL) and measurements were performed in triplicate at room temperature for 2 wk. Serum stability tests were conducted by suspending the nanoparticles in 100% FBS (Hyclone) with a final nanoparticle concentration of 1 mg/mL. The particles were first concentrated to 2 mg/mL and a concentrated 2× FBS was then added at equal volume. Absorbance measurements were conducted using an Infinite M200 multiplate reader. Samples were incubated at 37 °C with light shaking prior to each measurement. The absorbance at 560 nm was taken approximately every 30 min over a period of 4 h.

**Transmission Electron Microscopy Imaging.** The structure of the RBC-membrane-coated nanoparticles was examined using a transmission electron microscope. A drop of the nanoparticle solution at a concentration of 4 μg/mL was deposited onto a glow-discharged carbon-coated grid. Five minutes after the sample was deposited, the grid was rinsed with 10 drops of distilled water. A drop of 1% uranyl acetate stain was added to the grid. The grid was subsequently dried and visualized using a FEI 200KV Sphera microscope.

**Tissue Culture and Nanoparticle Endocytosis.** The human epithelial carcinoma cell line (HeLa) was maintained in RPMI medium 1640 (Gibco-BRL) supplemented with 10% fetal bovine albumin, penicillin/streptomycin (Gibco-BRL), L-glutamine (Gibco-BRL), MEM nonessential amino acids (Gibco-BRL), sodium bicarbonate (Cellgro), and sodium pyruvate (Gibco-BRL). The cells were cultured at 37 °C with 5% $CO_2$ and were plated in chamber slides (Cab-Tek II, eight wells; Nunc) with the aforementioned media. On the day of experiment, cells were washed with prewarmed PBS and incubated with prewarmed RPMI medium 1640 for 30 min before adding 100 μg of DMPE-RhB and DiD labeled RBC-membrane-coated PLGA nanoparticles. The nanoparticles were incubated with cells for 4 h at 37 °C. The cells were then washed with PBS 3 times, fixed with tissue fixative (Millipore) for 30 min at room temperature, stained with 4′,6-diamidino-2-phenylindole (DAPI, nucleus staining), mounted in ProLong Gold antifade reagent (Invitrogen), and imaged using a deconvolution scanning fluorescence microscope (DeltaVision System, Applied Precision). Digital images of blue, green, and red fluorescence were acquired under DAPI, FITC, and CY5 filters, respectively, using a 100× oil immersion objective. Images were overlaid and deconvoluted using softWoRx software.

**Protein Characterization Using SDS-PAGE.** The RBC ghosts, the RBC-membrane-derived vesicles, and the dialyzed RBC membrane-coated PLGA nanoparticles were prepared in SDS sample buffer (Invitrogen). The samples were then run on a NuPAGE® Novex 4-12% Bis-Tris 10-well minigel in 3-(*N*-morpholino) propanesulfonic acid running buffer using NovexSureLockXcell Electrophoresis System (Invitrogen). The samples were run at 150 V for 1 h, and the resulting polyacrylamide gel was stained in SimplyBlue (Invitrogen) overnight for visualization.

**Pharmacokinetics and Biodistribution Studies.** All the animal procedures complied with the guidelines of the University of California San Diego Institutional Animal Care and Use Committee. The experiments were performed on male ICR mice (6–8 wk) from Charles River Laboratories. To evaluate the circulation half-life of RBC-membrane-coated nanoparticles, 150 μL of DiD-loaded nanoparticles were injected into the tail vein of the mice. Twenty microliters of blood were collected at 1, 5, 15, 30 min, and 1, 2, 4, 8, 24, 48, and 72 h following the injection. The same dose of DiD containing PEG-coated lipid-PLGA hybrid nanoparticles and bare PLGA nanoparticles was also tested in parallel as controls. Each particle group contained six mice. The collected blood samples were diluted with 30 μL PBS in a 96-well plate before fluorescence measurement. Pharmacokinetics parameters were calculated to fit a two-compartment model and a one-way nonlinear model.

To study the biodistribution of the nanoparticles in various tissues, 18 mice received an injection of 150 μL of 3 mg/mL DiD-loaded nanoparticles through the tail vein. At each of the 24-, 48-, and 72-h time points following the particle injection, six mice were randomly selected and euthanized. Their livers, kidnesy, spleens, brains, lungs, hearts, and blood were collected. The collected organs were carefully weighed and then homogenized in 1 mL PBS. Total weight of blood was estimated as 6% of mouse body weight. The fluorescence intensity of each sample was determined by an Infinite M200 multiplate reader.

**ACKNOWLEDGMENTS.** This work was supported by the National Institute of Health (Grant U54CA119335) and by the National Science Foundation (Award CMMI 1031239).

1. Moghimi SM, Hunter AC, Murray JC (2001) Long-circulating and target-specific nanoparticles: Theory to practice. *Pharmacol Rev* 53:283–318.
2. Davis ME, Chen ZG, Shin DM (2008) Nanoparticle therapeutics: An emerging treatment modality for cancer. *Nat Rev Drug Discov* 7:771–782.
3. Peer D, et al. (2007) Nanocarriers as an emerging platform for cancer therapy. *Nat Nanotechnol* 2:751–760.
4. Yoo JW, Chambers E, Mitragotri S (2010) Factors that control the circulation time of nanoparticles in blood: Challenges, solutions and future prospects. *Curr Pharm Des* 16:2298–2307.
5. Geng Y, et al. (2007) Shape effects of filaments versus spherical particles in flow and drug delivery. *Nat Nanotechnol* 2:249–255.
6. Alexis F, Pridgen E, Molnar LK, Farokhzad OC (2008) Factors affecting the clearance and biodistribution of polymeric nanoparticles. *Mol Pharmacol* 5:505–515.
7. Knop K, Hoogenboom R, Fischer D, Schubert US (2010) Poly(ethylene glycol) in drug delivery: Pros and cons as well as potential alternatives. *Angew Chem Int Ed Engl* 49:6288–6308.
8. Jiang SY, Cao ZQ (2010) Ultralow-fouling, functionalizable, and hydrolyzable zwitterionic materials and their derivatives for biological applications. *Adv Mater* 22:920–932.
9. Yang W, Zhang L, Wang S, White AD, Jiang S (2009) Functionalizable and ultra stable nanoparticles coated with zwitterionic poly(carboxybetaine) in undiluted blood serum. *Biomaterials* 30:5617–5621.
10. Doshi N, Zahr AS, Bhaskar S, Lahann J, Mitragotri S (2009) Red blood cell-mimicking synthetic biomaterial particles. *Proc Natl Acad Sci USA* 106:21495–21499.
11. Tsai RK, Rodriguez PL, Discher DE (2010) Self inhibition of phagocytosis: The affinity of 'marker of self' CD47 for SIRPalpha dictates potency of inhibition but only at low expression levels. *Blood Cells Mol Dis* 45:67–74.
12. Merkel TJ, et al. (2011) Using mechanobiological mimicry of red blood cells to extend circulation times of hydrogel microparticles. *Proc Natl Acad Sci USA* 108:586–591.
13. Desilets J, Lejeune A, Mercer J, Gicquaud C (2001) Nanoerythrosomes, a new derivative of erythrocyte ghost: IV. Fate of reinjected nanoerythrosomes. *Anticancer Res* 21:1741–1747.
14. Cheng J, et al. (2007) Formulation of functionalized PLGA-PEG nanoparticles for in vivo targeted drug delivery. *Biomaterials* 28:869–876.
15. Tanaka M, Sackmann E (2005) Polymer-supported membranes as models of the cell surface. *Nature* 437:656–663.
16. Hochmuth RM, Evans CA, Wiles HC, McCown JT (1983) Mechanical measurement of red cell membrane thickness. *Science* 220:101–102.
17. Fang RH, Aryal S, Hu CM, Zhang L (2010) Quick synthesis of lipid-polymer hybrid nanoparticles with low polydispersity using a single-step sonication method. *Langmuir* 26:16958–16962.
18. Popielarski SR, Pun SH, Davis ME (2005) A nanoparticle-based model delivery system to guide the rational design of gene delivery to the liver. 1. Synthesis and characterization. *Bioconjug Chem* 16:1063–1070.
19. Goutayer M, et al. (2010) Tumor targeting of functionalized lipid nanoparticles: assessment by in vivo fluorescence imaging. *Eur J Pharm Biopharm* 75:137–147.
20. Xiao K, et al. (2009) A self-assembling nanoparticle for paclitaxel delivery in ovarian cancer. *Biomaterials* 30:6006–6016.
21. Gratton SE, et al. (2007) Nanofabricated particles for engineered drug therapies: A preliminary biodistribution study of PRINT nanoparticles. *J Control Release* 121:10–18.
22. Peracchia MT, et al. (1999) Stealth PEGylated polycyanoacrylate nanoparticles for intravenous administration and splenic targeting. *J Control Release* 60:121–128.
23. Simberg D, et al. (2007) Biomimetic amplification of nanoparticle homing to tumors. *Proc Natl Acad Sci USA* 104:932–936.
24. Oldenborg PA, et al. (2000) Role of CD47 as a marker of self on red blood cells. *Science* 288:2051–2054.
25. Gu F, et al. (2008) Precise engineering of targeted nanoparticles by using self-assembled biointegrated block copolymers. *Proc Natl Acad Sci USA* 105:2586–2591.
26. Avgoustakis K, et al. (2003) Effect of copolymer composition on the physicochemical characteristics, in vitro stability, and biodistribution of PLGA-mPEG nanoparticles. *Int J Pharm* 259:115–127.
27. Zhang L, Zhang L (2010) Lipid-polymer hybrid nanoparticles: Synthesis, characterization and applications. *Nano LIFE* 1:163–173.
28. Sengupta S, et al. (2005) Temporal targeting of tumour cells and neovasculature with a nanoscale delivery system. *Nature* 436:568–572.
29. Valencia PM, et al. (2010) Single-step assembly of homogenous lipid-polymeric and lipid-quantum dot nanoparticles enabled by microfluidic rapid mixing. *ACS Nano* 4:1671–1679.
30. Liu J, Stace-Naughton A, Jiang X, Brinker CJ (2009) Porous nanoparticle supported lipid bilayers (protocells) as delivery vehicles. *J Am Chem Soc* 131:1354–1355.
31. van Schooneveld MM, et al. (2010) Imaging and quantifying the morphology of an organic-inorganic nanoparticle at the sub-nanometre level. *Nat Nanotechnol* 5:538–544.
32. Dodge JT, Mitchell C, Hanahan DJ (1963) The preparation and chemical characteristics of hemoglobin-free ghosts of human erythrocytes. *Arch Biochem Biophys* 100:119–130.
33. Zhang L, et al. (2008) Self-assembled lipid-polymer hybrid nanoparticles: A robust drug delivery platform. *ACS Nano* 2:1696–1702.
34. Waugh RE, Sarelius IH (1996) Effects of lost surface area on red blood cells and red blood cell survival in mice. *Am J Physiol* 271:C1847–1852.
35. Arnold MM, Gorman EM, Schieber LJ, Munson EJ, Berkland C (2007) NanoCipro encapsulation in monodisperse large porous PLGA microparticles. *J Control Release* 121:100–109.
36. Jacobs RL, Alling DW, Cantrell WF (1963) An evaluation of antimalarial combinations against plasmodium berghei in the mouse. *J Parasitol* 49:920–925.